Isotope effects on the dynamics properties and reaction mechanism in the CL(2P) + NH3 reaction: A QCT and QM study

ARTICLE *in* THEORETICAL CHEMISTRY ACCOUNTS · FEBRUARY 2013

Impact Factor: 2.23 · DOI: 10.1007/s00214-013-1349-5

5 AUTHORS, INCLUDING:

Manuel Monge-Palacios
University of Missouri
21 PUBLICATIONS **68** CITATIONS
SEE PROFILE

Cipriano Rangel
Universidad de Extremadura
27 PUBLICATIONS **318** CITATIONS
SEE PROFILE

Joaquin Espinosa-Garcia
Universidad de Extremadura
141 PUBLICATIONS **2,157** CITATIONS
SEE PROFILE

Theor Chem Acc (2013) 132:1349
DOI 10.1007/s00214-013-1349-5

REGULAR ARTICLE

Isotope effects on the dynamics properties and reaction mechanism in the $Cl(^2P) + NH_3$ reaction: a QCT and QM study

Manuel Monge-Palacios · Cipriano Rangel · Joaquin Espinosa-García · Hong Fu · Minghui Yang

Received: 28 September 2012 / Accepted: 6 February 2013

Abstract Isotope effects on dynamics properties and reaction mechanism in the title reaction, which evolve through deep wells in the entry and exit channels, were analysed using both quasi-classical trajectory and reduced dimensional quantum mechanical calculations, for collision energies in the range 3.0–10.0 kcal mol^{-1}, on an analytical potential energy surface (PES-2010) recently developed by our group. The analysis of different dynamics properties (reaction probability, product energy partitioning, and product rovibrational distributions) shows the reaction behaviour of the two reactions, $Cl + NH_3$ and $Cl + ND_3$, to be similar: direct mechanism, with a small percentage of indirect mechanisms, that is, trapping complex mediated. We find that the only dynamics property dependent on the isotope effect is the product scattering distribution. In particular, while the perdeuterated reaction favours backward scattering, the perprotio analogue favours forward scattering. This behaviour is related to the smaller maximum impact parameter for the perdeuterated reaction.

Keywords $Cl + NH_3$ reaction · Isotope effect · Reaction dynamics · Reaction mechanism

1 Introduction

The chemistry of the reaction of ammonia with chlorine atoms is very complex, with many intermediate fast reactions being involved [1]. Perhaps unsurprisingly therefore, the $Cl(^2P) + NH_3(v) \rightarrow HCl + NH_2$ hydrogen abstraction reaction has been little studied, either experimentally or theoretically. Only two experimental kinetics measurements have been reported [2, 3], and we know of only four theoretical studies [3–6]. The reaction is endothermic and very slow, but the most interesting characteristic is the presence of deep wells in the entry and exit channels which can influence the reaction dynamics.

In a very recent work [7], we constructed an analytical potential energy surface, PES-2010, for this reaction and its isotope analogues. This surface is based exclusively on high-level ab initio calculations. We found that the ab initio information used in the fit is well reproduced by the new PES-2010 surface, especially the barrier height and the depth of the wells, and that this surface reproduces the experimental forward rate constants in the common temperature range. However, to the best of our knowledge, no dynamics information about this reactive system is available, either experimental or theoretical, and only recently has our group begun a series of dynamics studies using quasi-classical (QCT) and quantum–mechanical (QM) calculations to analyse the role that these complexes in the entry and exit channels play in the dynamics and the atomic-level mechanisms [8, 9]. Due to the presence of the reactant well, we found different mechanisms of reaction

Manuel Monge-Palacios and Hong Fu contributed equally to this work.

Published as part of the special collection of articles derived from the 8th Congress on Electronic Structure: Principles and Applications (ESPA 2012).

M. Monge-Palacios · C. Rangel · J. Espinosa-García (✉)
Departamento de Química Física, Universidad de Extremadura, 06071 Badajoz, Spain
e-mail: joaquin@unex.es

H. Fu · M. Yang
State Key Laboratory of Magnetic Resonance and Atomic and Molecular Physics, Wuhan Institute of Physics and Mathematics, Chinese Academy of Sciences, Wuhan 430071, People's Republic of China

Published online: 19 February 2013

depending on the collision energy: indirect at low (<3 kcal mol^{-1}) and direct at high (>5 kcal mol^{-1}) collision energies [8].

To go deeper into the understanding of this reaction and the role of the isotopic substitution, in the present work, we describe a combined QCT/QM dynamics study of the deuterated analogue reaction, $Cl(^2P) + ND_3(v = 0) \rightarrow DCl + ND_2$, using the same analytical PES-2010 surface. By comparing the results with the perprotio system, we shall analyse the influence of the complexes in the entry and exit channels on the dynamics and the atomic-level mechanism. Unfortunately, as in the $Cl + NH_3$ reaction, neither experimental nor theoretical dynamics information is available for comparison.

The article is structured as follows. Section 2 briefly outlines the potential energy surface, and the energy and computational details of the quasi-classical trajectory (QCT) and reduced dimensionality quantum mechanical (QM) methods for the dynamics study of the deuterated reaction. Section 3 presents the QCT and QM dynamics results, together with a comparison with the perprotio reaction. This latter is re-analysed based on the new findings of the reduced dimensionality QM calculations which called into question the previous conclusions about the mechanism at very low energies [8]. Finally, the conclusions are presented in Sect. 4.

2 Theory and computational details

2.1 Potential energy surface

All calculations were performed on a potential energy surface (PES-2010) recently constructed by our group for the $Cl(^2P) + NH_3(v) \rightarrow HCl + NH_2$ gas-phase polyatomic reaction and its isotopic analogues [7]. The surface is symmetric with respect to permutation of the ammonia hydrogen atoms, a feature especially interesting for dynamics calculations. The functional form was developed in the cited work and therefore will not be repeated here. Basically, it consists of three LEP-type stretch terms (str), augmented by valence (val) bending terms, and a series of switching functions allowing the smooth change from pyramidal NH_3 to the planar NH_2 product in the hydrogen abstraction reaction. It depends on 32 adjustable parameters. As input data in the fitting process, we used exclusively very high-level ab initio calculations [CCSD(T) = FULL/aug-cc-pVTZ]. If one neglects the spin–orbit coupling, then electronic ^2P ground state of the chlorine atom is triply degenerate. Interaction with the NH_3 molecule removes this degeneracy, giving rise in general to three orthogonal states. In the Cs symmetry, the states are as follows: $1^2A'$, $2^2A'$, and $2^2A''$. Nevertheless, only the one with lowest energy ($1^2A'$) adiabatically correlates with the $HCl(X^1\sum^+) + NH_2$ (X^2) products. Thus, we shall focus attention on the ground state ($1^2A'$).

The PES-2010 has a reaction energy of 9.2 kcal mol^{-1}, and the transition state is located 'late' on the reaction path with a barrier height of 6.6 kcal mol^{-1}. In addition, it presents two deep wells—one in the entry valley, stabilised 7.2 kcal mol^{-1} with respect to the reactants, and another in the exit channel, stabilised 7.3 kcal mol^{-1} with respect to the products. This surface has been tested [7], finding good agreement with the available experimental data. Figure 1 shows the potential energy and the adiabatic changes (i.e., zero-point energy included) along the reaction paths for the $Cl(^2P) + ND_3$ and $Cl(^2P) + NH_3$ for comparison. While the reactant wells present similar stabilities, the adiabatic barriers, the products wells, and the endothermicity are 1.3 kcal mol^{-1} higher for the deuterated reaction. Note however that with a higher barrier height, the deuterated reaction presents a deeper reactant well. Obviously, these differences could have consequences on the kinetics and dynamics.

2.2 Available energy and reaction threshold

Formally, the total energy (zero-point energy included) available to reaction is

$$E_{avail} = E_{int,react} + E_{coll} \quad (1)$$

where $E_{int,react}$ and E_{coll} are, respectively, the internal energy of the reactants and the collision energy. For the endothermic $Cl(^2P) + ND_3(v = 0)/NH_3(v = 0)$ reactions, the minimum energy to open the deuterium/hydrogen abstraction reaction does not depend on the adiabatic barrier, 3.5/2.2 kcal mol^{-1}, but on the adiabatic reaction

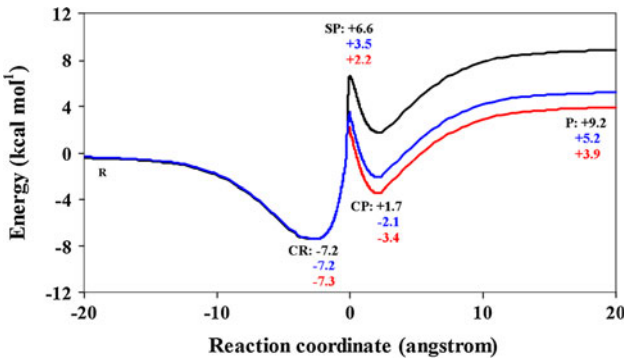

Fig. 1 Plots of the non-relativistic potential energy (*black line*) and adiabatic (i.e., zero-point energy included) profiles along the reaction path for the $Cl(^2P) + ND_3$ (*blue line*) and $Cl(^2P) + NH_3$ (*red line*) reactions using the PES-2010 surface. For each stationary point, the first entry corresponds to the potential energy along the path, the second to the adiabatic energy for the $Cl + ND_3$ reaction, and the third to the adiabatic energy for the $Cl + NH_3$ reaction. All values with respect to the reactants, level zero

energy, 5.2/3.9 kcal mol^{-1}, respectively, which is the reaction threshold in each reaction. Classically, one must expect that only encounters with E_{avail} above-the-reaction threshold, 5.2 kcal mol^{-1} for the perdeuterated reaction and 3.9 kcal mol^{-1} for the perprotio reaction, will result in products. However, in this particular reaction, these data merit more attention, as was extensively analysed in our previous paper [8]. Here, therefore, we present just a brief synthesis.

First, the experimental enthalpy of reaction is unknown and must be obtained from the corresponding enthalpies of formation, ΔH_f(0K). However, while the ΔH_f's of all the compounds are well established [10], the proposed experimental values of the NH_2/ND_2-free radical are a subject of serious controversy, with an uncertainty of ± 1.0 kcal mol^{-1} in accordance with the latest experimental value [11]. Second, the reactant NH_3/ND_3 rotational energy can be calculated theoretically from the equipartition energy, (3/2)RT, or sampled from a thermal distribution, as in the present paper in which a temperature of 300 K is used. Obviously, this rotational energy is available for reaction. At this temperature, (3/2)RT = 0.9 kcal mol^{-1}.

Therefore, given the reactant rotational energy and the experimental uncertainties in the enthalpy of reaction, it is very difficult to propose a minimum collision energy with which to surpass the reaction threshold. A reasonable theoretical approach is to suppose a lower limit for the collision energy. In our previous study on the $Cl + NH_3$ reaction, we use a value $\geq$2.5 kcal mol^{-1}, and in the present study for the $Cl + ND_3$ reaction, we propose a value $\geq$4.0 kcal mol^{-1}. Obviously, one expects that the experimental detection of products at the lower limit, if the interaction finally results in products, will present serious problems since the products' signal will be blurred by the experimental noise. Thus, these reactions represent a clear challenge experimentally at low energies.

2.3 Quasi-classical trajectory calculations

Quasi-classical trajectory calculations [12–14] were carried out using the VENUS96 code [15], customised to incorporate our analytical PESs. The accuracy of the trajectories was checked by the conservation of total energy and total angular momentum. The integration step was 0.1 fs, with an initial separation between the Cl atom and the ammonia centre of mass of 10.0 Å. Moreover, additional tests were performed at larger distances, 12.0 and 14.0 Å, finding no differences in final results. The trajectories were finished when the Cl–N distance was greater than 11.0 Å. As in the $Cl + NH_3$ reaction, at low collision energies, this large distance represents very long times of flight as compared with the high-energy regime. For direct comparison with the perprotio reaction, the vibrational energy corresponds to the ND_3 in its ground vibrational state, and the rotational energies were obtained by thermal sampling at 300 K from a Boltzmann distribution. The reactant collision energies considered ranged from 3.0 to 10.0 kcal mol^{-1}.

For each energy, the maximum value of the impact parameter, b_{max}, was determined by first calculating batches of 10,000 trajectories at fixed values of the impact parameter, b, systematically increasing the value of b until no reactive trajectories were obtained. This value varied depending on the collision energy, from 3.0 Å at 3.0 kcal mol^{-1} to 2.7 Å at 10.0 kcal mol^{-1}. Note that for the $Cl + NH_3$ reaction, the values in this range vary from 3.9 to 3.2 Å.

Then, batches of 200,000 trajectories were calculated for each collision energy, with the impact parameter, b, sampled from

$$b = b_{max} R^{1/2} \tag{2}$$

where R is a random number in the interval [0,1]. Moreover, to allow comparison with the QM calculations which were performed at $J = 0$, selected calculations on the PES-2010 surface were repeated with an impact parameter $b = 0$. In total, about 2×10^6 trajectories were run.

The reaction probability, $P_r = N_r/N_T$, is the ratio of the number of reactive trajectories to the total number of trajectories, while the reaction cross section is defined as

$$\sigma_r \pi b_{max}^2 (N_r/N_T) \tag{3}$$

Because of the large number of trajectories run, the sampling with respect to the impact parameter and rovibrational states is good enough to allow one to expect that the results do not depend on the averaging method. Therefore, Eq. (3) can be applied despite its simplicity.

It is well known that one of the difficulties with quasi-classical simulations is related to the question of how to handle the zero-point energy (ZPE) problem. Various strategies have been proposed to correct this quantum–mechanical effect, but no really satisfactory alternatives have emerged (see, for instance, Refs. [16, 17] and references therein). Here, we employed a pragmatic solution, the so-called passive method, which consists of running the trajectories with no quantum constraint to subsequently analyse the trajectories and discard those that are not allowed in a quantum mechanical world, even knowing that this method perturbs the statistics and can therefore lead to uncertainties in the dynamics study [18]. Recently, our group has analysed the ZPE problem in QCT calculations using full-dimensional QM results on the same PES as a target for the $H + NH_3$ reaction [19]. So, in Eq.(3), the correct determination of the number of reactive trajectories, N_r, and the total number of trajectories, N_T, has to be done having in mind the ZPE problem. So, we have three possible values of calculating N_r: counting all the reactive

trajectories (N_r^{all}), counting only those that lead to both products with vibrational energy above their ZPE, which is named histogram binning with double ZPE constraint, HB-DZPE, and counting only the trajectories that lead to the newly formed bond, HCl, with vibrational energy above its ZPE, following Thrular's [20] and Schatz's [21] suggestions, who suggested that the ZPE constraint should be applied just to the newly formed bond. We call this method histogram binning with ZPE-HCl constraint, HB-ZPE-HCl.

However, this way of removing trajectories from the N_r count without taking into account, the behaviour of the total ensemble of trajectories can lend erroneous results, because as mentioned above, it modifies the statistics [16, 18, 22]. So, here we count the total number of trajectories, N_T, in two ways. First, as it has been usual in the QCT literature, we consider the total number of trajectories ran in the calculation, N_T^{all}. In the second approach, N_T in Eq. (3) is replaced by the total number of trajectories minus the number of reactive trajectories whose final vibrational energy is below the ZPE of the two products or the H_2 product (depending on whether we use the HB-DZPE or HB-ZPE-H2 criterion), and minus the number of nonreactive trajectories whose final vibrational energy is below the ZPE of the NH_3 reactant. This number we call, N_T^*. Therefore, we have six counting methods for the calculations of the reaction probability, N_r/N_T, and therefore of the reaction cross section: N_r^{all}/N_T^{all}, $N_r^{HB\text{-}DZPE}/N_T^{all}$, $N_r^{HB\text{-}ZPE\text{-}HCl}/N_T^{all}$, N_r^{all}/N_T^*; $N_r^{HB\text{-}DZPE}/N_T^*$, $N_r^{HB\text{-}ZPE\text{-}HCl}/N_T^*$.

Taking the full-dimensional QM calculations as a target we found [19] that the best agreement was obtained with the $N_r^{HB\text{-}ZPE\text{-}HCl}/N_T^*$ approach. In the previous paper [8] on the Cl + NH_3, we used this criterion, and given that in the present paper, we study isotope effects on the Cl + NH_3 reaction, we use the same approach. So, possible errors in the counting methods can cancel out.

2.4 Quantum mechanical calculations

A seven-dimensional quantum dynamics model for the reaction X + YCZ_2 was employed in this work. The details of the method have been described elsewhere [23] and will only be briefly outlined here. For the Cl + ND3 reaction, Jacobi coordinates are employed to describe the motion of the system (Fig. 2). $\boldsymbol{R}$ is the vector from the centre of mass of ND_3 to the Cl atom; $\boldsymbol{r}$ is the vector from the centre of mass of ND_2 to the third D atom; q is the bond length of ND and is fixed at its equilibrium values; χ is the bond angle between the two ND bonds; and the vector $\boldsymbol{s}$ is the symmetry axis of the NH_2 group. The bending angle between vectors $\boldsymbol{R}$ and $\boldsymbol{r}$ is defined to be θ_1; φ_1 is the azimuth angle of the rotation of ND_3 around the vector $\boldsymbol{r}$; θ_2 is the bending angle between vectors $\boldsymbol{r}$ and $\boldsymbol{s}$; and φ_2 is the azimuth angle of the rotation of ND_2 around vector $\boldsymbol{s}$. The atomic masses are denoted as m_{Cl}, m_N, and m_D.

The model Hamiltonian for the Cl + ND_3 system is

$$\hat{H} = -\frac{1}{2\mu_R}\frac{\partial^2}{\partial R^2} - \frac{1}{2\mu_r}\frac{\partial^2}{\partial r^2} + \frac{(\hat{J}_{tot} - \hat{J})^2}{2\mu_R R^2} + \frac{\hat{l}^2}{2\mu_r r^2} + \hat{K}^{vib}_{ND_2} + \hat{K}^{rot}_{ND_2} + V(R, r, \chi, \theta_1, \phi_1, \theta_2, \phi_2) \quad (4)$$

where μ_R is the reduced mass of the Cl + ND_3, system and μ_r is the reduced mass of D + ND_2. The first two terms are the kinetic energy operators for R and r, respectively; $\hat{J}_{tot}$ is the total angular momentum operator of the system; $\hat{J}$ is the rotational angular momentum operator of ND_3; and $\hat{l}$ is the orbital angular momentum operator of atom Y with respect to ND_2. The last term $V(R, r, \chi, \theta_1, \phi_1, \theta_2, \phi_2)$ is the potential energy.

By fixing the ND bond lengths at their equilibrium values, the vibrational kinetic energy operator of the ND_2 bending vibration is

$$\hat{K}^{vib}_{ND_2} = -\frac{1}{\mu_1 q^2}\frac{1}{\sin\chi}\frac{\partial}{\partial\chi}\sin\chi\frac{\partial}{\partial\chi} + \frac{1}{\mu_2 q^2}\left(\frac{\cos\chi}{\sin\chi}\frac{\partial}{\partial\chi}\sin\chi\frac{\partial}{\partial\chi} + \sin\chi\frac{\partial}{\partial\chi}\right) \quad (5)$$

where $\mu_1 = m_N$ and $\mu_2 = m_N m_D/(m_N + m_D)$ are the reduced masses. The rotation of the ND_2 group is approximated to be decoupled from its vibrational motion and described by an asymmetric rigid rotor Hamiltonian, with the rotational constants $\{B_X, B_Y, B_Z\}$ varying with the bending angle χ.

$$\hat{K}^{rot}_{ND_2} = \frac{1}{2}(B_X + B_Y)\hat{j}^2 + \left[B_Z - \frac{1}{2}(B_X + B_Y)\right]\hat{j}_z^2 + \frac{1}{2}(B_X - B_Y)(\hat{j}_+^2 + \hat{j}_-^2) \quad (6)$$

where $\hat{J}$ is the angular momentum operator of the ND_2 group, $\hat{J}_Z$ is the z-component of $\hat{J}$, and $\hat{J}_+$ and $\hat{J}_-$ are the shift operators.

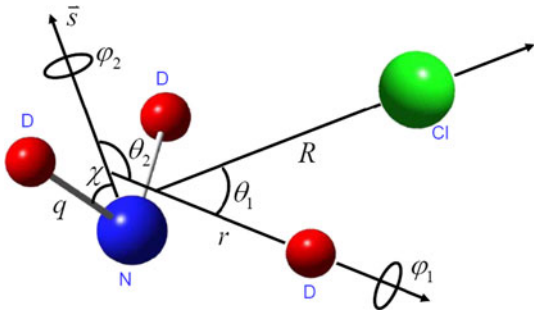

Fig. 2 Jacobi coordinates of the X + YCZ_2 model for the Cl + ND_3 reaction

Because of the double well in this reaction, we used an extremely large basis set in the work. In the L-shape technique used for coordinates R and r, a total of 480 basis sine functions ranging from 2.5 to 23.0 Bohr were used for the R basis set expansion with 410 nodes in the interaction region. The range of r was set to be from 1.0 to 21.0 Bohr to include the well in the product side, and 5 and 140 basis functions were used in the asymptotic and interaction regions, respectively. For the ND_2 bending mode, 1 PODVR (potential-optimised discrete variable representation) node was used. The size of the rotational basis function set is controlled by the parameters, $J_{max} = 48$, $l_{max} = 30$, $j_{max} = 18$, and $k_{max} = 18$. After considering parity and C_{2v} symmetry, the size of the set of rotational basis functions was 54, 979, and the number of nodes for the integration of the rotational basis set was 654, 493. The size of the total basis function set was 3.175×10^9 and the number of nodes was 3.78×10^{10}. The dividing surface was defined at $r = 3.5$ Bohr. Due to the deep well in the entry channel and the heavy mass of the Cl atom, the entire propagation time was 25,000 a.u. with a step size of 10 a.u. for the reaction to converge from ND_3 initially in its vibrational ground state. In sum, the time-dependent quantum mechanical calculations provide total reaction probabilities as a function of the translational energy for $J_{tot} = 0$.

Before ending this section, we believe it is interesting to note that, compared with other polyatomic reactions, the Cl + NH3 reaction is very complex due to its two deep van der Waals complexes on the reactant and on the product sides. The QCT approach, although classical in nature, considers all the reaction coordinates and produces very useful information.

Also, the computational cost makes it difficult to carry out a full-dimensional QM calculation for this heavy system and complex reaction, although we actually have developed the full-dimensional method. The reduced dimensional QM model used in the present paper is reasonable since the values of the spectator bond length (N–H) and bond angle (H–N–H) are almost same in the geometries of the reactant and transition state. The reduced QM calculation is thus able to explore quantum effects in this reaction at an affordable computational cost and is an useful complement to the full-dimensional QCT calculations.

3 Results and discussion

3.1 Reaction probability: influence of the reactant well and mechanism of reaction

Figure 3 shows the reaction probability as a function of the collision energy for the Cl + ND_3 reaction, together with the Cl + NH_3 reaction for comparison, using the QCT and QM calculations on the same PES-2010 surface. With this plot, we shall analyse the dynamics method, the influence of the reactant well, and the mechanism of reaction.

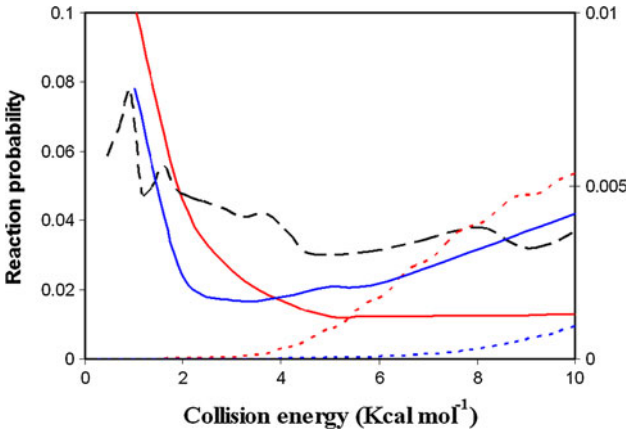

Fig. 3 Reaction probability as a function of the collision energy (kcal mol^{-1}) using the PES-2010 surface for the Cl + ND_3 reaction (*blue lines*) and Cl + NH_3 reaction (*red lines*). *Solid lines*: QCT calculations (b = 0); *dashed lines*: QM calculations ($J = 0$). We also include the wrong 7D-QM calculations for the Cl + NH_3 reaction for completeness (*black-dashed line*). Note that for a clearer discussion, the scales in the *right* and *left axis* are different: Only the QCT (*red-solid line*) and the old 7D-QM (*black-dashed line*) results are represented on the *left axis*

First, it is important to note that we have found a mistake in the previous 7D-QM calculations for the Cl + NH_3 reaction [8], and the peak in the reaction probability at low energies is wrong in the reduced dimensionality quantum dynamics calculations. In particular, the parameter to define the dividing surface was wrongly selected. In that paper, the parameter was wrongly set to be $r = 2.2$ Bohr and therefore in the entry channel and before of the saddle point ($r = 2.5$ Bohr), where r is defined as the distance between the third atom and the centre of mass of NH_2. Thus, some wavepackets did not pass through the saddle point were wrongly considered. In the present paper, all calculations set the flux surface to be $r = 3.5$ Bohr which is in the product channel.

The new 7D-QM calculations for the Cl + NH_3 reaction show a very different behaviour, where the reaction probability increases smoothly with collision energy from the reaction threshold. Thus, the new QM calculations show the typical behaviour of a reaction with barrier, and neither resonances nor another quantum effects are observed below the reaction barrier. Therefore, the increase in reaction probability at low energies obtained with the QCT calculations in that work [8], due to repeated collisions between the Cl and NH_3 reactants in the entry valley, was really an artefact of the QCT method based on the ZPE violation, where all trajectories appear with the vibrational energy in the NH_2 product below its ZPE, which is quantum

mechanically forbidden. The well in the entry channel yields an unphysical vibrational → translational energy transfer, which artificially favours the use of this energy to promote the reaction, and the classical above-the-threshold reaction occurs even when the collision energy is below the quantum–mechanical threshold to reaction.

Second, due to the higher threshold for the perdeuterated reaction with respect to the perprotio ones (Fig. 1), the reactivity is smaller at all collision energies. This result agrees with the kinetic isotope effects found in our previous kinetics study [7] using the same surface, which ranged from 9.2 at 300 K to 1.4 at 2000 K. Thus, the deuteration diminishes the reactivity because the threshold is higher ($\sim$1.3 kcal mol^{-1}) due to the different ZPEs.

Third, for the Cl + ND_3 reaction, the QCT probability presents slight increases in reactivity with collision energy from the threshold of reaction, with slight increases also at lower energies. Is this behaviour at low energies a real effect or an artefact of the QCT calculations as in the case of the Cl + NH_3 reaction? The 7D-QM calculations also give a very small reactivity, indicating that few wavepackets pass though the reaction threshold, although there is no enhancement of reactivity at low collision energies. Therefore, the QCT reactivity at low energies is an artefact of the method (as in the Cl + NH_3 reaction), and the QM results are more realistic.

To look more deeply into the QCT results at low energies, we performed a detailed analysis of the trajectories. At low energies, we observed all reactive trajectories to appear with the vibrational energy in the ND_2 product below its ZPE, an effect known as ZPE violation. Thus, part of the leaked vibrational energy is used to promote the reaction, and the classical above-the-threshold reaction occurs even when the collision energy is below the quantum–mechanical threshold to reaction (the zero-point energy corrected threshold). In other words, although QCT assumes classical motion along the reaction path, there is a possibility for the reaction to occur by lowering the vibrational energy below the ZPE, even though there is not enough energy to surpass the threshold. In the analysis of trajectories in the low-energy regime, we observed that orthogonal motions on the reaction path (vibrational modes of the ND_3–ND_2 evolution) are transformed into translational energy along the path, and that this $V \rightarrow T$ transfer was used to overcome the threshold. Therefore, the ND_2 product appears with vibrational energy below its ZPE, which is quantum mechanically forbidden. This is the reason for the significant values of the reaction probability at low energies observed in Fig. 3, both for the Cl + ND_3 and for the Cl + NH_3 reactions. The larger enhancement for the Cl + NH_3 reaction is due to lower collision energies, permitting a larger number of collisions between the Cl and NH_3 reactants in the entry valley, which favours the unphysical $V \rightarrow T$ energy transfer. Therefore, the reactivity at low energies is an artefact of the QCT calculations, which is confirmed by the QM results.

For comparison purposes, we examined the influence of another two counting methods—the VEQMT [24] and the VEQMTc [25] approaches. Using the VEQMT approach, we obtained no reactive trajectory in the energy range considered, 3–10 kcal mol^{-1}, confirming that this approach is too restrictive, as has previously been noted [25]. In this sense, the VEQMT approach is similar to our DZPE counting method. When the less stringent VEQMTc approach is used, it should be taken into account that the zero-point energy of the product complex is 0.2 kcal mol^{-1} higher than the ZPE of the products, so that no reactive trajectory should be expected with this counting method. Indeed, an energy of 10.0 kcal mol^{-1} is required to obtain only 2 % of the reactive trajectories. For this system, therefore, the VEQMT and VEQMTc approaches are both too restrictive. Another non-active scheme [24] would be to require the internal energy of each product molecule to be larger than or equal to its ZPE (internal energy quantum mechanical threshold (IEQMT) scheme), which is a priori less demanding than VEQMT. In fact, we obtained no reactive trajectories in the energy range 3–5 kcal mol^{-1}, while at 10.0 kcal mol^{-1}, we obtain only 3 % of reactive trajectories. Therefore, for the present reaction, the IEQMT scheme follows being too restrictive. These results show that there is no unambiguous way to fix the leakage problem of classical mechanics, so that the only solution is via quantum mechanics [25].

Finally, we also examined the influence of the impact parameter. All the QCT calculations were re-run with b_{max} (instead of $b = 0$). The variation of the reaction probability with the collision energy was similar in shape to the $b = 0$ case and so is not shown here. Therefore, the behaviour with energy and the possible mechanisms are independent of the choice of impact parameter. After this comparison with QM calculations, in the rest of this communication, the value used for the QCT calculations will be b_{max}.

3.2 Nature of the trajectories and atomic-level reaction mechanisms: comparison with the Cl + NH_3 reaction

In order to determine the nature of the trajectories and the atomic-level mechanism, we performed an analysis of the individual reactive trajectories over the wide collision energy range considered, comparing them with the Cl + NH_3 system previously studied [8]. We made a distinction between direct and indirect (i.e., trapping complex mediated) mechanisms. The former involves a very brief encounter between the reactants and is the most likely in the high-energy regime. In the latter, the influence of the

Table 1 Atomic-level mechanism as a function of the collision energy for $Cl(^2P) + ND_3$ and $Cl(^2P) + NH_3$ reactions using the PES-2010 surface

Collision energy[a]	Direct trajectories (%)[b]		Indirect trajectories (%)[c]	
	$Cl + ND_3$	$Cl + NH_3$	$Cl + ND_3$	$Cl + NH_3$
3.0	–	85	–	15
4.0	90	100	10	0
5.0	100	100	0	0
10.0	100	100	0	0

[a] In kcal mol^{-1}

[b] Percentages calculated with respect to the total of reactive trajectories

[c] Total percentage of indirect trajectories (calculated with respect to the total of reactive trajectories), that is, trajectories that enter the reactant and/or product complex regions

wells in the entry and/or exit channels is important, and indeed is the dominant factor in the low-energy regime. Table 1 summarises the influence of the energy regime on the reaction mechanism, presenting the percentages of the reactive trajectories which occur via direct and indirect mechanisms for each reaction. The data at collision energies of 3.0 and 4.0 kcal mol^{-1} for NH_3 and ND_3 reactions correspond, respectively, to the limit of the respective low-energy regime threshold.

To gain insight into the reaction mechanism, Fig. 4 shows typical cases of the evolution of the broken bond N–D (dashed line) and formed bond D–Cl (solid line) distances as a function of time. In the direct or impulse-type mechanism (Fig. 4a), $E_{coll} > 4.0$ kcal mol^{-1}, the Cl collides with ND_3 and forms the DCl product which immediately recoils away. In the indirect mechanism (Fig. 4b–d), 10 % of reactive trajectories at $E_{coll} = 4.0$ kcal mol^{-1}, the situation is more complicated since the trajectories pass through the regions of the complexes. Two basic types of trajectories were found—those that enter the reactant complex region (Fig. 4b), and those that enter the product complex region (Fig. 4c). In the former case, the Cl and ND_3 reactants undergo several collisions in the entry channel, with different energy transfers between T, R, and V. The reactive system does not fly apart following these collisions, and after a certain time, the trajectory suddenly 'finds' the way towards the products. The complex in the entry channel thus allows repeated encounters between the reactants before the formation of the products, explaining the reaction probability at low energies. In the latter case (Fig. 4c), once formed, the DCl and ND_2 products do not fly apart. Instead, they undergo several collisions in the exit channel, usually associated with rotation of the DCl product. After a certain time (whose magnitude depends on the trajectory), the products separate. Obviously, a combination of these two kinds of trajectory (Fig. 4b,c) is also possible, as was indeed found in the visualisation of individual reactive trajectories (Fig. 4d). At low collision energies, these indirect reactions (Fig. 4b–d) represent about 10 % of the trajectories, while at high collision energies, they represent practically 0 %. Classically, these nearly trapped trajectories, similar to the motion of a spring or to the popular 'yo-yo' toy, are a straightforward consequence of the presence of the reactant well. This behaviour of the direct and indirect trajectories is similar to that observed for the $Cl + NH_3$ reaction [8], although at higher collision energies in the perdeuterated case (see Table 1).

However, considering the arguments given in Sect. 3.1 about the possible artefact of the QCT calculations at low energies, confirmed with the reduced dimensionality QM

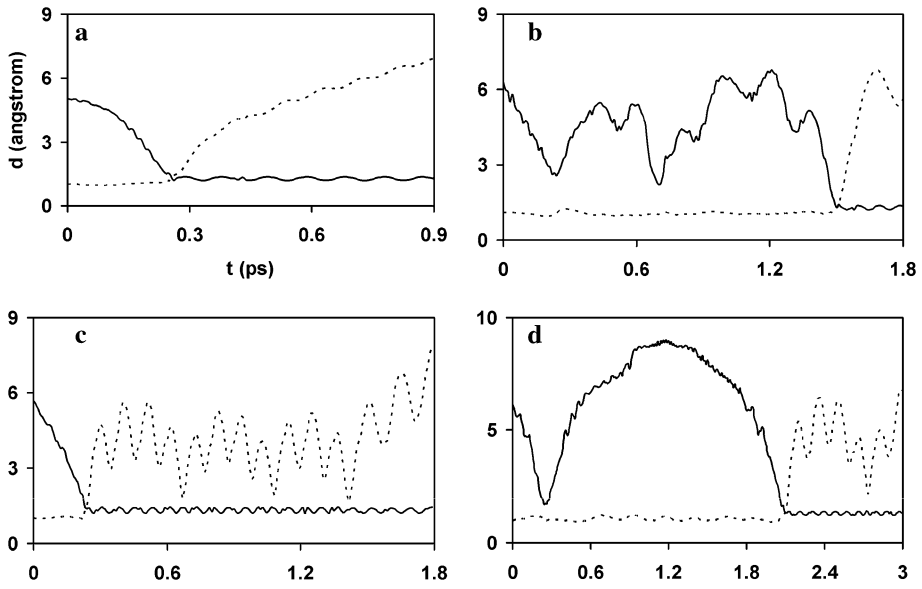

Fig. 4 Representative plots of different reaction mechanisms, shown as the evolution of the N–D (*dashed line*) and D–Cl (*solid line*) distances as a function of time (ps), using the PES-2010 surface: **a** direct trajectory; **b** indirect trajectory in the entry channel; **c** indirect trajectory in the exit channel; and **d** indirect trajectory in the entry and exit channels

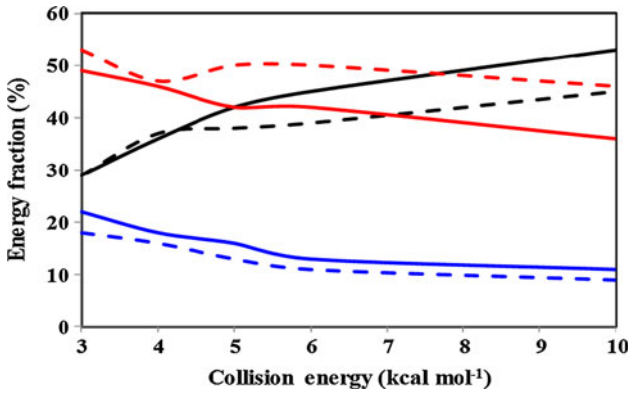

Fig. 5 QCT results using the PES-2010 surface for the Cl + ND_3 reaction (*solid lines*) and Cl + NH_3 reaction (*dashed lines*) for the average translation energy, f_{trans}, (*black line*), and internal energy of the products, $f_{int}(ND_2/NH_2)$, (*blue line*) and f_{int}(DCl/HCl), (*red line*), in percentages, as a function of the collision energy

calculations, one must be very careful about the importance of the indirect mechanism in these reactions.

3.3 Product energy partitioning

Although the product energy partitioning is an experimental property that is easily measurable and could represent a test of our theoretical results (PES and dynamic methods), unfortunately neither are data on this property currently available. Figure 5 shows, in percentages, the average translational energy, f_{trans}, and internal energy of the products, $f_{int(ND2)}$ and $f_{int(DCl)}$, as functions of the collision energy, together with the QCT results for the Cl + NH_3 reaction for comparison. The values and behaviour of the two reactions are similar—the product internal energies decrease with collision energy, while the translational energy increases by the same amount. This similarity in behaviour indicates that the partitioning of the energy in the products is fairly insensitive to the isotope effect and to the depth of the reactant well.

3.4 Product rovibrational distributions

At all the collision energies analysed, 3.0–10.0 kcal mol^{-1}, the ND_2 and DCl products appeared essentially in their respective vibrational ground state, $v = 0$.

The QCT vibrationally resolved DCl ($v = 0$) rotational distributions for the Cl + ND_3 reaction are plotted in Fig. 6 for two collision energies –low and high: 4.0 and 10.0 kcal mol^{-1}—together with the results for the Cl + NH_3 reaction for comparison. The two reactions present similar shapes, with the diatomic product appearing with a broad and hot rotational distribution. Note, however, that the QCT methods tend to give rotational distributions that are hotter and broader than experiment and the results

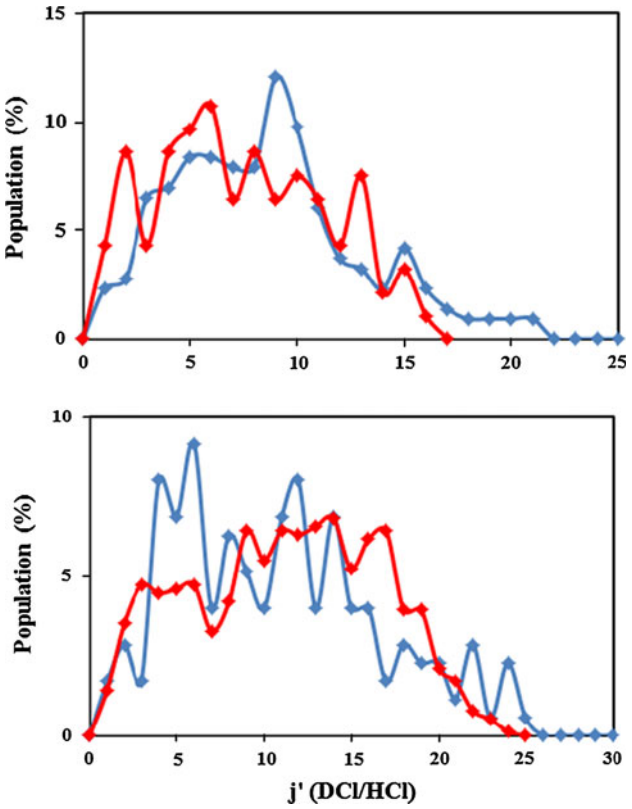

Fig. 6 QCT vibrationally resolved DCl/HCl($v = 0$) rotational distributions using the PES-2010 surface for the Cl + ND_3 reaction (*blue lines*) and Cl + NH_3 reaction (*red lines*), for two collision energies—low and high: 4.0 and 10.0 kcal mol^{-1} (*upper* and *lower panels*, respectively)

of quantum–mechanical methods [26–31], an effect which is an artefact of these classical methods. Given the linear transition state for this reaction, which generates little torque during an impulsive release, a priori one might have expected a colder rotational distribution. Thus, the hot rotational distribution for the two reactions could be related to the existence of deep wells in the entry and exit channels. The attractive interaction in the reactant well provides more torque and therefore more rotational excitation, while the attractive interaction in the product well may provide a more pronounced torque on the two separating products, and a greater randomization of the rotational energy, thereby explaining the hot and broad rotational distribution. Unfortunately, there are neither experimental nor other theoretical results available for comparison.

3.5 Product angular distribution

The product angular distribution is doubtless one of the most sensitive dynamics properties with which to test the quality of the surface and to examine the role of intermediate complexes in the reaction. To analyse the isotope effect, we consider two collision energies: the threshold of reaction (4.0 kcal mol^{-1}

for the perdeuterated reaction, and 2.5 kcal mol^{-1} for the perprotio ones), and an energy clearly above this threshold, 10.0 kcal mol^{-1}, in both cases. The QCT angular scattering distribution of the diatomic product (DCl or HCl) with respect to the incident chlorine atom (obtained as the differential cross section, DCS, which was fitted using the Legendre moment method [32]) is plotted in Fig. 7.

In the threshold of reaction (Fig. 7, upper panel), while the Cl + NH_3 reaction showed a forward–backward shape, the Cl + ND_3 reaction presented a more isotropic behaviour. This is clearly related to the indirect trajectories: 38 versus 10 %. The indirect mechanism is characterised by a forward–backward distribution, as is typical of reactions occurring via a deep minimum. Thus, due to the smaller collision energy for the Cl + NH_3 reaction (and consequently the greater importance of the indirect mechanism), the effect of the entry valley is more pronounced.

At 10.0 kcal mol^{-1}, the collision energy is enough to surpass the reaction threshold, the direct trajectories predominate (100 % for both reactions), and the behaviour is very different (Fig. 7, lower panel). While the Cl + NH_3 reaction showed a sideways-forward distribution, associated with a stripping mechanism with high impact parameters, the Cl + ND_3 reaction shows a sideways-backward scattering, associated with lower impact parameters. Indeed, at 10.0 kcal mol^{-1}, the b_{max} values are 3.2 and 2.7 Å, respectively, for the NH_3 and ND_3 systems. To analyse more clearly the influence of the impact parameter, Fig. 8 shows the opacity function (reaction probability vs. impact parameter) in the two energy regimes analysed, threshold (upper panel) and high (lower panel). It is known that the contribution of smaller impact parameters leads to backward-scattered products. In both energy regimes, the Cl + ND_3 reaction presents a larger contribution of small impact parameters, favouring backward scattering.

In summary, the product scattering distribution is the only dynamics property analysed which is strongly

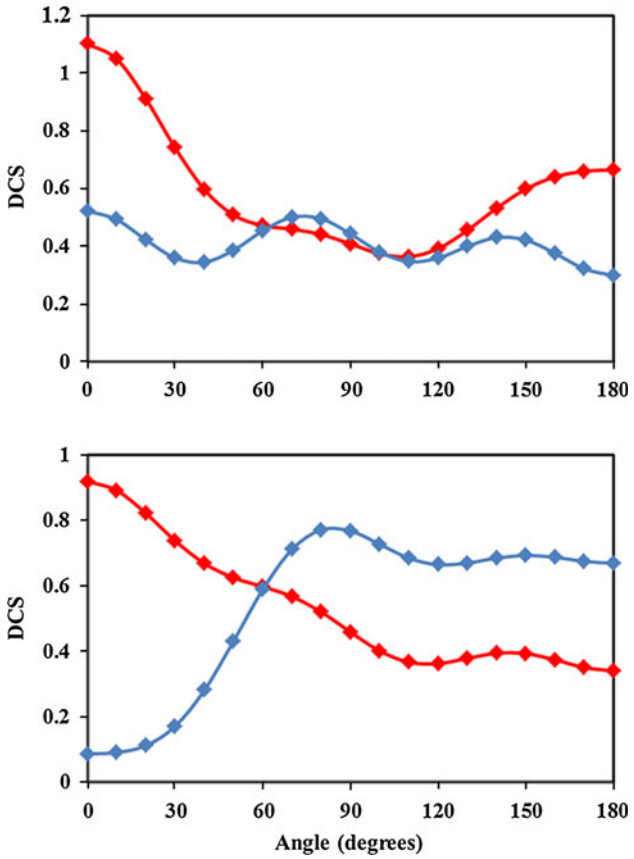

Fig. 7 QCT results using the PES-2010 surface for the DCl product angular distribution (with respect to the incident Cl) for the Cl + ND_3 → DCl + ND_2 reaction (*blue lines*) and for the HCl product angular distribution for the Cl + NH_3 → HCl + NH_2 reaction (*red lines*). *Upper panel* low collision energy—4.0 kcal mol^{-1} for the Cl + ND_3 reaction and 2.5 kcal mol^{-1} for the Cl + NH_3 reaction. *Lower panel* high collision energy—10.0 kcal mol^{-1} for both reactions

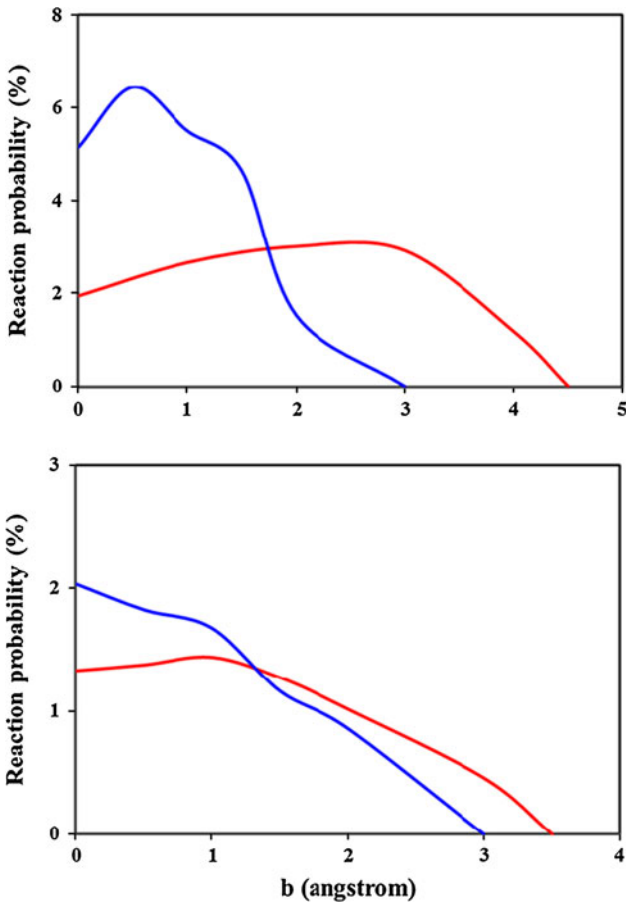

Fig. 8 Opacity function (reaction probability vs. impact parameter) using the PES-2010 surface for the Cl + ND_3 reaction (*blue lines*) and Cl + NH_3 reaction (*red lines*). *Upper panel* low collision energy—4.0 kcal mol^{-1} for the Cl + ND_3 reaction and 2.5 kcal mol^{-1} for the Cl + NH_3 reaction. *Lower panel* high collision energy—10.0 kcal mol^{-1} for both reactions. In each case, the distributions are normalised so that the area under the common levels is the same

dependent on the isotope effect, and it seems to indicate that there are different mechanisms for the two isotopes. Clearly more theoretical and new experimental studies will be needed to understand these differences.

4 Conclusions

We have described an extensive state-to-state dynamics study performed on an analytical potential energy surface (PES-2010) recently developed for the gas-phase abstraction reaction $Cl(^2P) + ND_3 \rightarrow DCl + ND_2$, using reduced dimensionality quantum mechanical (7D-QM) and quasi-classical trajectory (QCT) calculations. In the QCT study, the zero-point energy problem was explicitly considered to avoid leakage along the trajectories, and the collision energy ranged from 3.0 to 10.0 kcal mol^{-1}. The dynamics results were compared with those for the perprotio reaction in order to analyse the isotope effect.

The QCT product energy partitioning showed that the translational energy increases with collision energy, while the internal energy of the products, DCl and ND_2, decreases by the same amount. At all the collision energies studied, the DCl and ND_2 products appeared practically in their respective vibrational ground states, while the $DCl(v = 0)$ rotational distribution was broad and hot. Given that this reaction presents a linear transition state geometry, the hot distribution could be related to the existence of wells in the entry and exit channels. The attractive interaction in these wells could provide a more pronounced torque and greater randomization of the rotational energy. These two dynamics properties—product energy partitioning and rovibrational distributions—showed similar behaviour to the case of the $Cl + NH_3$ reaction, indicating that they are insensitive to the isotope effect.

With respect to the variation of the reaction probability with the collision energy, the $Cl + ND_3$ and $Cl + NH_3$ reactions present similar behaviour, with the probability increasing smoothly from the reaction threshold, which is the typical behaviour for reactions with a barrier. Hence, the effect of the entry valley is negligible for these reactions. We find that the product scattering distribution is the only dynamics property strongly dependent on the isotope effect, and it seems to indicate that there are different mechanisms for the two isotopes. The smaller maximum impact parameter for the perdeuterated reaction favours backward scattering, as compared to forward scattering for the perprotio analogue. In sum, the deuteration (through the ZPE effect) changes the shape of the adiabatic energy profile, possibly modifying the reaction mechanism.

Unfortunately, no experimental dynamics information is available for this polyatomic system, whether perprotio or perdeuterated. We therefore trust that this and similar theoretical studies might encourage future experimental research into this complex reaction and its mechanism, especially at low energies.

Acknowledgments This work was partially supported by the Gobierno de Extremadura (Spain), the Fondo Social Europeo (Project No. IB10001), and the National Science Foundation of China (Projects No. 20921004, 21073229 and 20833007). MMP thanks the Gobierno de Extremadura (Spain) for a scholarship. Many calculations were carried out on the LUSITANIA computer at Computaex (Spain).

References

1. Miller JA, Bowman CT (1989) Prog Energy Combust Sci 15:287
2. Westenberg AA, DeHaas N (1977) J Chem Phys 67:2388
3. Gao Y, Alecu IM, Hsieh PC, Morgan BP, Marshall P, Krasnoperov LN (2006) J Phys Chem A 110:6844
4. Kondo S, Tokuhashi K, Kaise M (2000) J Hazard Mat A 79:77
5. Xu ZF, Lin MC (2007) J Phys Chem A 111:584
6. Monge-Palacios M, Espinosa-Garcia J (2010) J Phys Chem A 114:4418
7. Monge-Palacios M, Rangel C, Corchado JC, Espinosa-Garcia J (2012) Int J Quantum Chem 112:1887
8. Monge-Palacios M, Yang M, Espinosa-Garcia J (2012) Phys Chem Chem Phys 14:4824
9. Monge-Palacios M, Corchado JC, Espinosa-Garcia J (2012) Phys Chem Chem Phys 14:7497
10. Chase MW, Davis CA, Downey JR, Frurip DJ, McDonald RA, Syverud AN (1985) JANAF Thermochemical tables, J Phys Chem Reference Data vol 14, Suppl 1
11. Song Y, Qian XM, Lan KC, Ng CY, Liu J, Chen W (2001) J Chem Phys 115:2582
12. Porter RN, Raff LM (1976) In: Miller WH (ed) Dynamics of molecular collisions, part B, Ed. Plenum Press, New York
13. Truhlar DG, Muckerman JT (1979) In: Bernstein RB (ed) Atom-molecules collision theory. Plenum Press, New York
14. Raff LM, Thompson DL (1985) In: Baer M (ed) Theory of chemical reaction dynamics, vol 3. CRC Press, Boca Raton
15. Hase WL, Duchovic RJ, Hu X, Komornicki A, Lim KF, Lu Dh, Peslherbe GH, Swamy KN, van de Linde SR, Varandas AJC, Wang H, Wolf RJ (1996) VENUS96: a general chemical dynamics computer program. QCPE Bull. 16:43
16. Varandas AJC (1994) Chem Phys Lett 225:18
17. Duchovic RJ, Parker MA (2005) J Phys Chem A 109:5883
18. Guo Y, Thomson DL, Sewell TD (1996) J Chem Phys 104:576
19. Corchado JC, Espinosa-Garcia J, Yang M (2011) J Chem Phys 135:014303
20. Gray JN, Garrett BC, Truhlar DG (1979) J Chem Phys 70:5921
21. Kudla K, Schatz GC (1993) Chem Phys 175:71
22. Bonnet L (2008) J Chem Phys 128:044109
23. Yang M, Corchado JC (2007) J Chem Phys 126:214312
24. Varandas AJC (1993) J Chem Phys 99:1076
25. Varandas AJC (2001) Chem Phys Lett 340:62
26. Gerrity DP, Valentini JJ (1984) J Chem Phys 81:1298
27. Kliner DAV, Rinnen KD, Zare RN (1990) Chem Phys Lett 166:107
28. Dean BD, Ayers JD, Fernandez-Alonso F, Zare RN (2001) J Phys Chem A 105:2228
29. Dean BD, Ayers JD, Fernandez-Alonso F, Zare RN (2002) J Chem Phys 116:6634
30. Pomerantz AE, Ausfelder F, Zare RN, Althorpe SC, Aoiz FJ, Bañares L, Castillo JF (2004) J Chem Phys 120:3244
31. Xiao T, Bowman J, Duff JW, Braunstein M, Ramachandran B (2005) J Chem Phys 122:014301
32. Truhlar DG, Blais NC (1977) J Chem Phys 67:1532